Low frequency seismic sensor based on GPS interferometry

A. Dalla Torre[1], A. Caporali[1,2] and N. Praticelli[2]

[1] *Centro Interdipartimentale di Studi e Attività Spaziali CISAS G. Colombo, Università degli Studi di Padova, Italy*

[2] *Dipartimento di Geologia, Paleontologia e Geofisica, Università degli Studi di Padova, Italy*

(Received March 19, 2004; accepted September 1, 2004)

ABSTRACT The ground deformation before, during and after a seismic event contains valuable information to understand the mechanics of earthquakes. Traditional seismometry is based upon the integration of an acceleration signal delivered by an elastically suspended mass near the resonance frequency. This approach is optimal for relatively high frequency deformations. However, there is evidence that non-negligible deformations take place at much lower frequencies, and a suitable detection device is therefore needed. To better understand and experiment with a non-accelerometric seismic sensor sensible to low frequency perturbations (10 Hz and below), we have developed a prototype seismometer based on GPS interferometry. Our breadboard consists of six NovAtel/CMC single frequency SmartAntennas configured in a two-dimensional array with spacing ranging between 1 and 5 meters. We have developed a real time software to log data from the six receivers and to compute and interpret the phase differences between pairs of receivers. The knowledge of the nominal coordinates of the receivers is used to solve and to monitor the integer ambiguities. We demonstrated that the data processing at each epoch, from this net, leads to relative coordinates between the receivers with root-mean-square repeatability between 4 and 8 mm horizontally and between 13 to 19 mm vertically. The resulting horizontal strain rates range from 0.8×10^{-3} to 8×10^{-3} 1/s at a frequency of 1 Hz. The sensor is therefore effective only for large earthquakes (magnitude ≥ 5.9 and 7.5 for angular separations of 1° and 10° respectively). The precision of the results is limited mainly by multipath. The effect of multipath can be mitigated using a calibration signal optimized for the site where the sensor is placed.

1. Introduction

Traditional seismographs are composed by a measuring system (seismometer), a time reference and data-recording module. A seismometer is traditionally made up of an inertial system formed by a test mass, a spring and a dumping element. For this reason the seismogram does not deliver an exact representation of the ground motion: its response is strongly affected by the frequency of the incoming signal relative to the resonance frequency of the instrument. More precisely, the response of a seimometer tends to be out of phase with ground motion.

Ground motion spans from 0.000023 Hz of the Earth tides to over 200 Hz for earthquakes. The dynamic range spans from 10^{-10} m for a magnitude 2 earthquake to 0.1 m for a magnitude 8 earthquake (Stein and Wysession, 2003).

The design of a seismometer is constrained by the contrasting need to amplify the signal and to scan a broad range of frequencies and amplitudes.

Conventional passive "pendulum" seismometers are generally in use only for high frequency with ranges centered on approximately 50 Hz. The maximum signal amplification is obtained using electromagnetic seismometers in which the mass is coupled with a coil that is moved by the ground motion inside a magnetic field. The voltage across the coil is proportional to the mass velocity. The electromagnetic seismometers are used for low frequencies (< 0.5 Hz) or, with lower amplification, for high frequency ranges. The maximum dynamic ranges and frequency ranges (1/300 Hz – 10 Hz) are obtained with digital force-feedback electromagnetic seismometers. The response curve of some force-feedback electromagnetic seismometers is shown in Fig. 1 (Stein and Wysession, 2003).

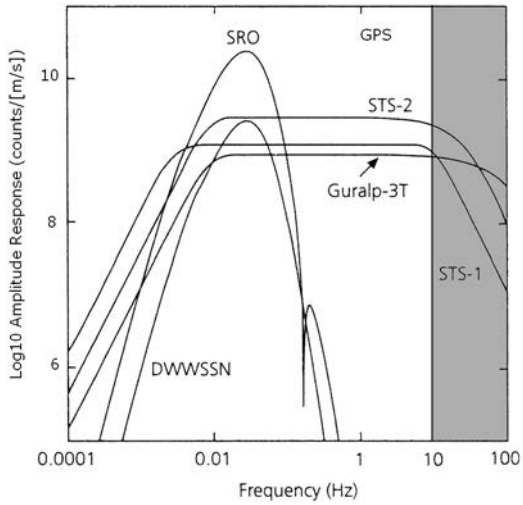

Fig. 1 - Frequency domain instrument responses for several types of seismometers. The SRO (Seismic Research Observatory) and the DWSSN (Digital World Wide Standardized Seismograph Network) sensors have responses peaked at long periods and so do not record high-frequency signals. The STS1, STS2 and Gurlap3T sensors are broadband seismometers with a flat response over a wide range of frequencies (Stein and Wysession, 2003). The GPS seismometer works for frequencies below 10 Hz.

With low-cost and high-performance GPS receivers, multi-antenna sensors with two or more antennas in a given configuration may provide an alternative and cheap way to measure deformations. This is obtained thanks to the phase differentiation for phases recorded simultaneously by the receivers; using this approach the coordinates of one side of the baseline are computed relatively to the other side. The response of the instrument requires no amplification and therefore one expects no frequency-dependent distorsion. The combined use of GPS geodetic techniques and seismic recordings show a strong correlation between the seismic events and the slow, relative position variation between pairs of GPS stations. Fig. 2 shows an example of this correlation (Rogers and Dragert, 2003). The figure shows that seismic events that seem to be apparently episodic, correspond to abrupt coordinate variations and that in the period between two contiguous seismic events the coordinate variations were continuous and well bound by GPS measurements.

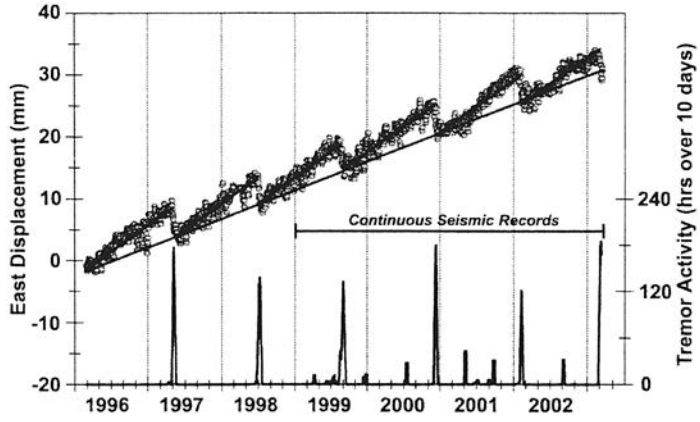

Fig. 2 - Correlation between the variation of the east coordinate of the ALBH (Victoria) permanent GPS station and the seismic activity in the Cascadia (Alaska) subduction zone axis. Dots show antenna east displacements (left axis). In the bottom part of the plot, the tremor activity is shown in hours over 10 days (right axis). The activity is represented by tremors with the main frequencies between 1 and 5 Hz. The periods with higher concentration of tremors correspond to abrupt changes in the east coordinates of the ALBH station, which is within 100 km from the source region. The geometry of the locked and transition zones associated with the Juan de Fuca Plate subduction has a N-NW orientation which implies that displacements are expected mostly in the E-W direction (Rogers and Dragert, 2003).

It would be desirable that displacements such as those shown in Fig. 2 were detected in real time, and immediately correlated with local seismic activity. However, the instrumentation needed for this purpose is still at a very early stage of development. Ge (1999), Ge et al. (2000) and Turner (2002) have demonstrated that the use of pairs of GPS receivers in real time kinematic mode allows ground oscillations at the centimeter level (~13 mm) with frequencies of some Hz (2.3 and 4.3 Hz) to be detected. In this context, the development of a prototype GPS sensor capable of monitoring in real time low frequency deformations finds its justification.

After a discussion of the signal structure and of the algorithms we present the preliminary results with 6 receivers and discuss the perspectives of operational use of this instrument.

2. GPS measurements

The carrier phase measurement Φ between a GPS satellite and a receiver is modelled as follows:

$$\Phi = \frac{\rho}{\lambda} + \frac{c}{\lambda}\Delta\delta + N - \frac{d_{ion}}{\lambda} + \frac{d_{trop}}{\lambda} + \varepsilon \qquad (1)$$

where Φ is expressed in cycles at the λ wavelength. N is the ambiguity of the measure (the integer number of cycles from its emission to its reception), $\Delta\delta$ contains the receiver and satellite clock offset and ε contains the residual errors, including multipath.

The data processing is based on the single differences between receivers for each satellite A tracked.

$$\Delta\Phi^{A} = \frac{\Delta\rho}{\lambda} + \frac{c}{\lambda}\Delta\tau + N^{A} - \frac{\Delta d_{ion}}{\lambda} + \frac{\Delta d_{trop}}{\lambda} + \varepsilon^{A} \qquad (2)$$

$\Delta\tau$ is the relative clock offset of the receivers. The first order model of the single differences for short enough baselines assumes that there is negligible horizontal ionospheric and tropospheric gradient:

$$\Delta\Phi^{A} = \frac{\vec{b}\cdot\hat{s}^{A}}{\lambda} + \frac{c\Delta\tau}{\lambda} + N^{A} + \varepsilon^{A} \qquad (3)$$

where $\vec{b}$ is the baseline vector and $\hat{s}^{A}$ is the line of sight unit vector to satellite A.

Eq. (3) is represented in Fig. 3, whereby, knowing the position of the satellites ($\hat{s}^{A}$) and after the resolution for the ambiguity term N^{A} ($N^{A} = N_1$-N_2, where 1 and 2 refer to the two receivers), we can determine the baseline length and orientation ($\vec{b}$) in space. This approach has been used to develop GPS interferometric attitude sensors by Caporali (2001) and Caporali et al. (2003).

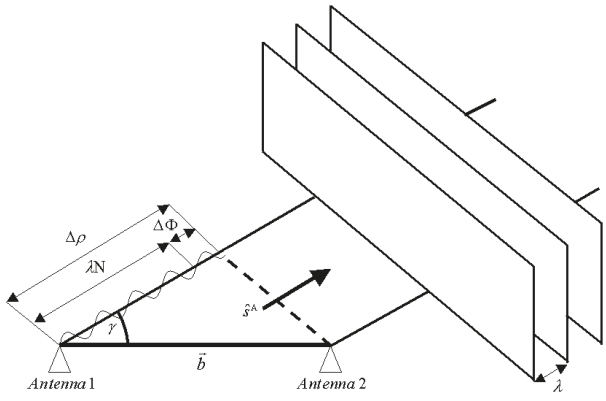

Fig. 3 - Phase single differences scheme. Given the navigation satellites position in sky s^{A} and after the solution for the ambiguity term N^{A}, the length and the orientation of the baseline b can be determined.

The single differences of phase must be differentiated again to remove the relative drift of the clocks. Phase observations received by pairs of receivers and transmitted by pairs of satellites are differentiated. A hub satellite (H) has to be defined, for example, as the one with higher elevation. The double difference between receivers and the A and H satellites is

$$\nabla\Delta\Phi^{AH} = \Delta\Phi^{A} - \Delta\Phi^{H} = \frac{\vec{b}\cdot(\hat{s}^{A} - \hat{s}^{H})}{\lambda} + N^{AH} + \varepsilon^{AH} \qquad (4)$$

where N^{AH} is the difference between the ambiguities of the two satellites ($N^{AH} = N^{A}$-N^{H}) and ε^{AH} is the difference between their noises ($\varepsilon^{AH} = \varepsilon^{A}$-$\varepsilon^{H}$). The receiver clock term which was present in Eq. (3) is now absent in Eq. (4).

3. Single baseline determination

The components of the baseline between a pair of receivers is determined by solving the double difference Eq. (4) for all the satellites in view, tracked at both antennas. Additional unknowns are the n-1 ambiguities N^{AH}, where n is the number of common navigation satellites. This solution is found at each epoch and, clearly, there are more unknowns than equations. The ambiguities are integer multiples of the wavelength (19 cm) and therefore can be pre-estimated because the knowledge of the system geometry is known a priori. Hence, after pre-elimination of ambiguities we are left with n-1 equations and 3 unknowns. This process of pre-elimination of the ambiguities must be repeated at every epoch independently of the other epochs due to the possibility that cycle slips modify the values of one or more ambiguities.

The double differenced phase, corrected for the integer ambiguities, enter the normal equations which will be solved by Least Squares.

The normal equations relate the residuals of the double differences of phase y to the vector x containing the azimuth *az*, the elevation *el* and the baseline length b:

$$y = \mathrm{A}x+\varepsilon \tag{5}$$

where A is the matrix of the partials of the Double Differences relative to the azimuth, the elevation and the length (BAE reference system), x is the array of the corrections to be applied to the length, the azimuth and the elevation, ε is the noise term. Assuming non-correlated observations, the use of the Least Square Solution approach leads to:

$$\mathrm{A}^{\mathrm{T}}y = \mathrm{A}^{\mathrm{T}}\mathrm{A}x \tag{6}$$

To be precise, double difference data are correlated and the correlation depends on the way the double differences are constructed. However, we will ignore this detail in the following although the calculation does take into account this correlation.

4. Solution for the basic triangular module

In order to study the deformation of large surfaces, the GPS network is resolved into triangular modules with a GPS antenna at each vertex. One defines two baselines and the angle between them for each module. Therefore, each module solution is given by the combination of two single baseline solutions with the constraint imposed by the knowledge of the angle between them. This solution leads to the adjusted coordinates of two vertices of the triangle.

The knowledge of the azimuth, of the elevation and of the length of the two baselines is combined with the knowledge of the geometry of the system using a Least Square Solution approach.

With reference to the normal equation [Eq. (5)], the x vector is now a 6-dimensional vector which contains the corrections to the components of the baselines in the north-east-up (NEU) system. The y vector contains the pre-fit residuals of the single baselines where the knowledge of the angle is added:

$$y_{(n1+n2+1)} = \cos(angle_{12}) - \frac{b_1 \cdot b_2}{|b_1||b_2|} \tag{7}$$

where n_1 and n_2 are the number of double differences for each baseline, $angle_{12}$ is the angle between the baselines b_1 and b_2. If, for example, 6 navigation satellites are observed by each receiver, $n_1 = n_2 = 5$ and the number of double differences is 10. Considering that the angle between the two baselines is approximately known we have a total of 11 equations and 6 unknowns. Therefore the structure of the normal equation for a triangle is given in Fig. 4.

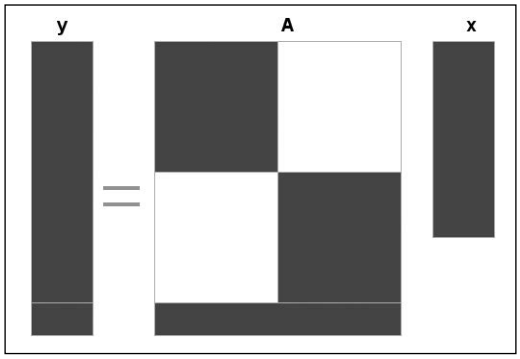

Fig. 4 - Normal equations for the combination of the single baseline solutions. The partial derivative matrix is made up of three parts: the two upper blocks are the partial derivatives for the single baselines while the lower block is the knowledge of the system geometry (angle between the vectors). The bound and its partial derivative "connect" the single solutions. The white parts are 3x3 null matrices.

5. Low-frequency GPS seismometer

A small prototype of the GPS seismometer has been set up on the roof of the CISAS (Centro Interdipartimentale di Studi e Attività Spaziali) building in Padova as an intermediate step in the development of a larger (a few square kilometers) and denser network. A net with baselines up to 10 meters has been studied.

Six NovAtel/CMC antennas embedded with the Allstar® receiver (1 Hz sampling rate) have been placed on the roof of the building of our institution and have been connected with a PC with 15 m long cables through the serial port with the RS-232 communication protocol.

In order to communicate simultaneously with all the receivers, a USB serial port multiplier (up to eight) by Quatech has been adopted (see Fig. 5).

Fig. 5 - Quatech USB serial port multiplier.

Fig. 6 shows a map of the antennas' position. In Table 1, the a priori coordinates of the antennas are given. A picture of the prototype of the seismic sensor is given in Fig. 7.

The adjusted coordinates of two of the three vertices with reference to the third of given coordinates are computed for each epoch and for each elementary module.

A software capable of communicating with the receivers through the serial ports has been realized. The software gives the user the possibility of tuning some parameters of the sensor and visualizing the adjusted coordinates of the antennas using a graphical interface in real time.

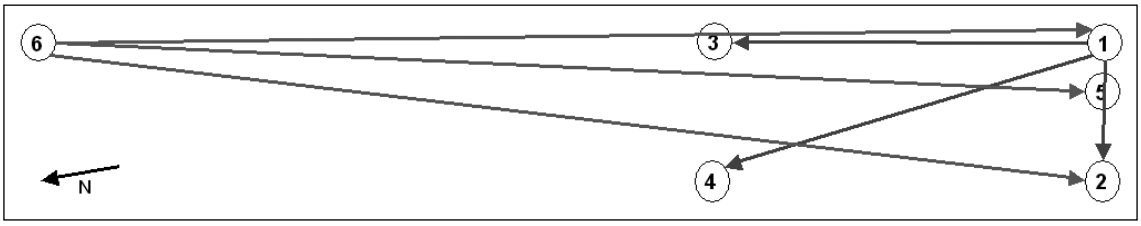

Fig. 6 - Map of the 6 GPS antennas. The antenna coordinates are given in Table 1. In our tests, four triangular modules have been considered: two modules with antenna 1 as the reference antenna (134 and 124) and two with antenna 6 (615 and 652).

Fig. 7 - Prototype of the seismic sensor.

Table 1 - A priori coordinates of the GPS antennas computed using the GPSurvey software in static mode with PADO (IGS and EUREF networks) as reference GPS station.

Antenna	Coordinate X $ECEF_{[m]}$	Coordinate Y $ECEF_{[m]}$	Coordinate Z $ECEF_{[m]}$
1	4388881.375	924556.209	4519590.838
2	4388881.204	924555.183	4519591.214
3	4388879.790	924556.867	4519591.992
4	4388879.698	924555.934	4519592.348
5	4388881.341	924556.023	4519590.902
6	4388877.660	924557.730	4519593.916

6. Results and implementation issues

Some static tests have been done in order to evaluate the stability and the repeatability of the solutions. The tests were done on January 21, 2004 and lasted for 4 hours for triangles 134 and 124 and 2 hours for triangles 615 and 653. A sampling rate of 1 Hz has been used. The sampling rate is limited only by the maximum sampling rate of the receivers in use (receivers with sampling rates up to 20 Hz are available).

In the case under investigation, four of the possible triangular modules (see Fig. 6) have been considered. These triangles are: 134, 124, 615 and 652 (the first number is the reference antenna of known coordinates). For each triangle, given the coordinates of one of the vertices, the coordinates of the other vertices are computed for each epoch. Each solution is independent from the previous ones. The output contains the ECEF (Earth Centered Earth Fixed) Cartesian coordinates of two of the GPS antennas and their displacement from the nominal position in the NEU system. Figs. 8 and 9 show the NEU displacements. Each figure refers to a different reference antenna (antenna 1 and antenna 6 respectively). Table 2 contains the adjusted coordinates of the GPS antennas with the root-mean-square (r.m.s.) repeatability computed by this approach while Table 3 contains the r.m.s. of the displacement solutions.

Table 2 - Adjusted coordinates of the GPS antennas with their r.m.s. repeatability.

Triangle	Antenna	$X_{[m]}$	$\sigma_{X[m]}$	$Y_{[m]}$	$\sigma_{y[m]}$	$Z_{[m]}$	$\sigma_{Z[m]}$
134	3	4388879.789	0.008	924556.871	0.006	4519591.987	0.008
	4	4388879.679	0.007	924555.934	0.009	4519592.338	0.011
124	2	4388881.202	0.005	924555.186	0.005	4519591.211	0.007
	4	4388879.679	0.007	924555.933	0.008	4519592.338	0.011
615	1	4388881.382	0.010	924556.206	0.007	4519590.840	0.012
	5	4388881.346	0.012	924556.024	0.007	4519590.903	0.012
652	5	4388881.346	0.011	924556.024	0.007	4519590.903	0.013
	2	4388881.207	0.013	924555.182	0.011	4519591.210	0.011

A seismic sensor validation has been obtained by comparing its results with the results from the commercial software GPSurvey® by Trimble®. Both software have been used with the same set of observation data. In Table 4, the results obtained in real time are compared with the results obtained in post-processing using GPSurvey®. As already said the seismic sensor gives a solution for each second while a static survey with GPSurvey® processes all the data in a unique solution.

Table 3 - R.m.s. repeatability of the GPS antennas computed NEU displacements.

Triangle	Antenna	$\sigma_{N[m]}$	$\sigma_{E[m]}$	$\sigma_{U[m]}$
134	3	0.005	0.006	0.013
	4	0.005	0.006	0.013
124	2	0.008	0.006	0.014
	4	0.005	0.006	0.013
615	1	0.005	0.005	0.017
	5	0.005	0.004	0.019
652	5	0.005	0.004	0.019
	2	0.008	0.006	0.014

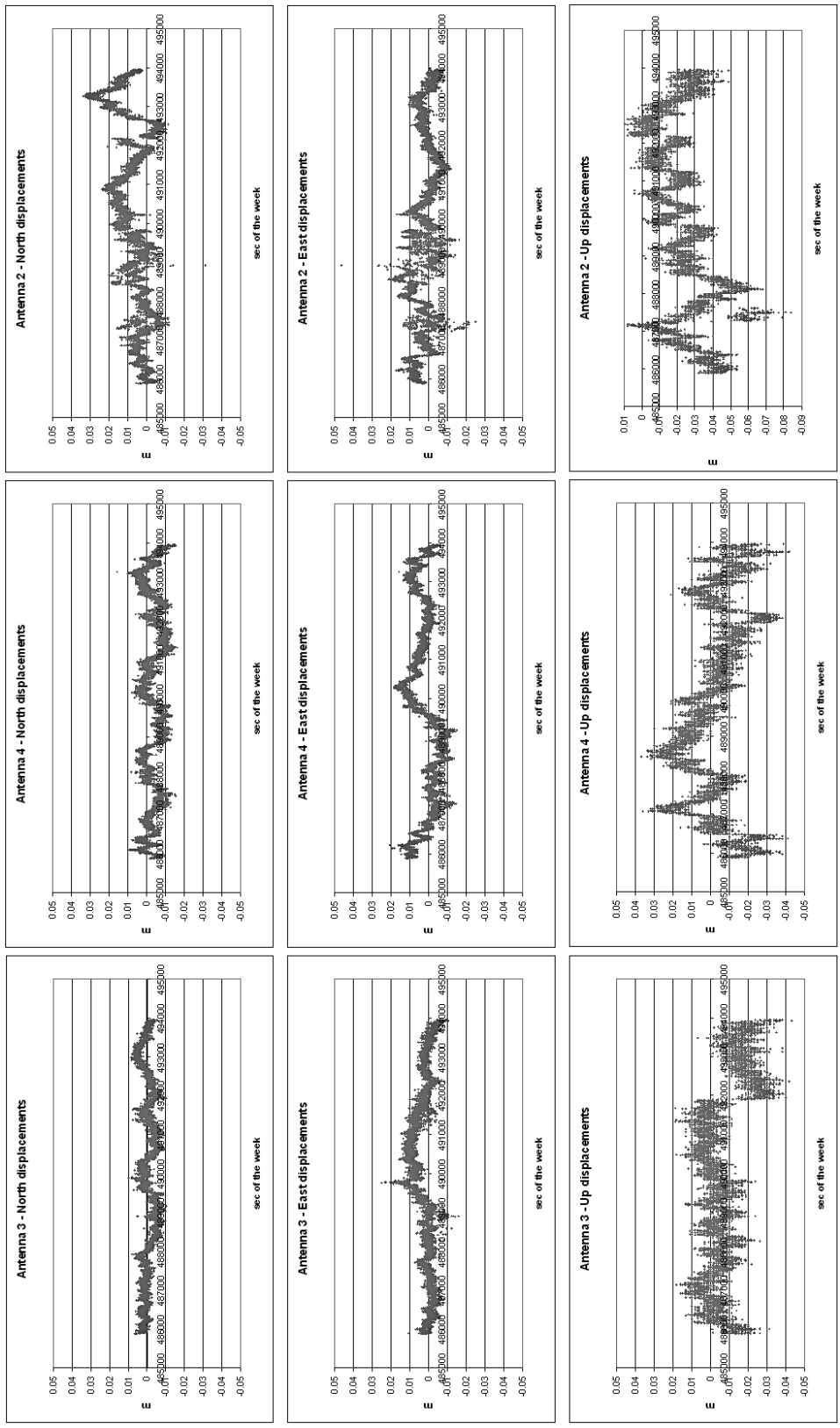

Fig. 8 - North, east and up displacements of antennas 3, 4 and 2 computed using the triangular modules 134 and 142. Antenna 1 is the reference antenna.

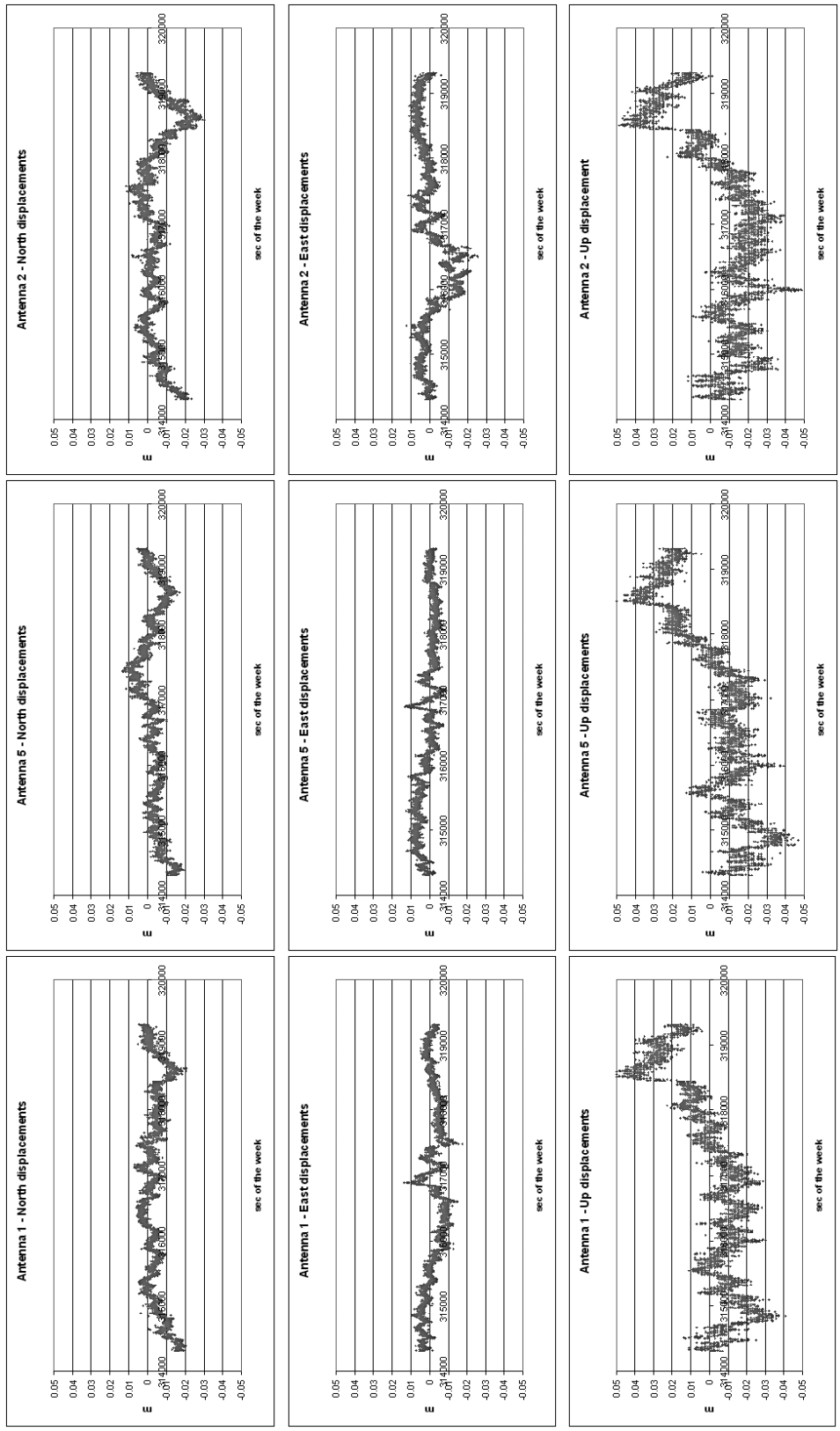

Fig. 9 - North, east and up displacements of the antennas 1, 5 and 2 computed using the triangular modules 615 and 652. Antenna 6 is the reference antenna.

Because the error is integrated over several hours the standard deviation computed with GPSurvey are lower than in our calculation where we have the r.m.s. of epochwise estimates.

Table 4 - Comparison between the baselines computed using the GPS seismic sensor and the baselines computed using the GPSurvey® software (between brackets). The uncertainties are intended as r.m.s. repeatability in our case and formal errors in GPSurvey.

	Azimut [deg]	σ_{az} [deg]	Elevation[deg]	σ_{el} [deg]	Length [m]	σ_{lun} [m]
1-2	298.90 (298.80)	0.17 (0.03)	-0.05 (-0.31)	0.41 (0.11)	1.102 (1.105)	0.005 (0.004)
1-3	28.26 (28.36)	0.16 (0.01)	-4.87 (-5.03)	0.31 (0.05)	2.067 (2.068)	0.005 (0.004)
1-4	2.02 (2.02)	0.21 (0.008)	-3.42 (-3.70)	0.29 (0.03)	2.281 (2.276)	0.008 (0.007)
6-1	206.50 (206.47)	0.09 (0.005)	1.65 (1.61)	0.17 (0.008)	5.064 (5.062)	0.004 (0.001)
6-5	208.72 (208.73)	0.1 (0.005)	1.58 (1.60)	0.19 (0.008)	5.057 (5.057)	0.005 (0.001)
6-2	218.89 (218.82)	0.11 (0.005)	1.57 (1.55)	0.19 (0.008)	5.137 (5.136)	0.005 (0.001)

The results of the static test show that the system is stable and repeatible between 4 and 8 mm r.m.s horizontally and between 13 and 19 mm vertically. Residual sistematic errors are given by multipath and have characteristic frequencies between 0.001-0.0025 Hz. This range agrees with the theoretical computation by Ge (1999) who identified it as a characteristic range for multipath 0.0008-0.02 Hz. The minimum observable displacement does not depend on the sampling rate since each solution is independent from the previous one.

The detectable horizontal strain rates resulting from the coordinates r.m.s. range from 8×10^{-4} to 8×10^{-3} 1/s at a frequency of 1 Hz using to the equation

$$strain\ rate = \frac{\Delta l}{l\Delta t} \tag{8}$$

where l and Δl are the length and the length variation respectively, Δt is the time interval between observations.

The order of magnitude of the displacements associated to the surface waves, according to the surface wave magnitude formula is (Stein and Wysession, 2003)

$$\begin{aligned} M_S &= \log\left(\frac{A}{T}\right) + 1.66 \log D + 3.3 \quad \text{or} \\ M_S &= \log A_{20} + 1.66 \log D + 2 \end{aligned} \tag{9}$$

where the first form is general and the second uses the amplitude of Rayleigh waves with a period of 20 s, which is often the largest in amplitude. A is the ground motion in microns, T is the wave period in seconds and D is the distance in degrees. Using the Rayleigh waves equation and a ground motion of 8 mm we obtain a limit magnitude of 7.5 with $D = 10°$ and 5.9 with $D = 1°$, such that we can hope to detect only large earthquakes with epicentre not too far from the instrument. Further studies need to be done to design the sampling rate and antenna spacing precisely, in consideration of seismic waves of large enough amplitude to produce a measurable displacement.

The potential for monitoring the propagation of surface ruptures is very important. This is a low frequency measurement not achievable with traditional seismometers and taking place on a relatively large area, at least for large earthquakes.

We are currently working on the possibility of predicting multipath using the fact that the constellation of satellites repeats regularly and that the reflecting surfaces near the array remain the same with time.

We plan to monitor the response of this prototype sensor to discover the oscillatory perturbations by displacing the antennas, for example using a vibrating table. The final device will eventually be scaled to accommodate the wavelength, typical of seismic events.

In order to show that it is possible to monitor length variations, we will generate oscillations of the antennas to verify the sensor's functionality in kinematic conditions.

An important issue in the development of the GPS seismometer will be the design of the GPS antennas network. For a signal, with a period of 1 s travelling at 5.5 km/s the wavelength is 5.5 km which means that the maximum distance between the antennas will be at least that large. This will pose communication problems that can be solved, for example, using radio links.

The antennas' grid does not need to be exactly regular, but the more regular it is, the better, as for all grids. Regular spacing lowers correlations of the estimated parameters. The nearly square architecture can be stacked to cover irregular areas, and the individual solutions from each quadrangular sensor can be combined as for a trigonometric network.

We plan to investigate the sensitivity of the array to the direction of the incoming wave by exploiting the correlation between changes in coordinates of the antennas and the orientation of the baselines formed by them. Earthquake location could also be improved by correlating the direction of the incoming waves at several such arrays.

REFERENCES

Caporali A.; 2001: *Solving your attitude problem: basic direction sensing with GPS*. GPS World, **12 (3)**, 44-50.

Caporali A., Dalla Torre A. and Praticelli N.; 2003: *Interferometric attitude and direction sensor using GPS carrier phase data*. Reports on Geodesy, **2 (65)**, 173-193.

Ge L.; 1999: *GPS seismometer and its signal extraction*. In: Proc. 12th Int. Tech. Meeting of the Satellite Division of the U.S. Inst. Of Navigation GPS ION'99, Nashville, Tennessee, 14-17 Sep. 1999.

Ge L., Han S., Rizos C., Ishikawa Y., Hoshiba M. and Yoshida Y.; 2000: *GPS Seismometers with up to 20 Hz sampling rate*. LETTER Earth Planet Space, **52**, 881-884.

Rogers G. and Dragert H.; 2003: *Episodic tremor and slip on the cascadia subduction zone: the chatter of silent slip*. SCIENCE, **300**, 1942-1943.

Stein S. and Wysessien M.; 2003: *An introduction to seismology. Earthquakes and Earth structure*. Blackwell Publishing, Oxford U.K., 498 pp.

Turner L.; 2002: *What's shaking? Earthquake trials test networked RTK*. GPS World, **13 (4)**, 16-22.

Corresponding author: Andrea Dalla Torre
CISAS G. Colombo, Università degli Studi di Padova
Via Venezia 15, 35131 Padova, Italy
phone: +39 0498276849 / 0498272054; e-mail: andrea.dallatorre@unipd.it